

# Correlation effects between turbulence and the conversion rate of pulverized char particles

Jonas Krüger<sup>\*,a</sup>, Nils Erland L. Haugen<sup>a,b</sup>, Terese Løvås<sup>a</sup>

<sup>a</sup>*Department of Energy and Process Engineering, Norwegian University of Science and Technology Kolbjørn Hejes vei 1B, NO-7491 Trondheim, Norway*

<sup>b</sup>*SINTEF Energy Research, N-7465 Trondheim, Norway*

---

## Abstract

The effect of turbulence on heterogeneous reactions on the surface of char particles embedded in a turbulent oxidizer, consisting of oxygen and carbon-dioxide, is in this work studied numerically. It is shown that for small Damköhler numbers (**Da**), the char conversion rates are somewhat *increased* by the turbulence. This is found to be due to the increased mass transfer rate to the char particle surface that is caused by the turbulence-induced relative velocity between the char and the oxidizer. For large Damköhler numbers, however, the char conversion rate is strongly *reduced* due to particle clustering. This reduction is explained by the fact that when particles are clustered in densely populated particle clusters, the transfer of oxygen to the particles in the centre of the clusters is reduced since the oxygen is consumed by the particles closer to the external surface of the cluster. At the same time, high concentrations of oxygen exist in the voids between the particle clusters. This oxygen can not take part in the conversion of the char until it is transported to the char surface. The effects of turbulence on the heterogeneous reaction rates are furthermore modelled based on Direct Numerical Simulation (DNS) data for a simplified reacting gas particle system.

*Key words:* Reacting multiphase flow; Particle clustering; Heterogeneous combustion; Direct Numerical Simulation; Char; Turbulence;

---

\*Corresponding Author: jonas.kruger@ntnu.no

## 1. Introduction

Numerical simulations are an important tool in predicting the performance, and planning the operation, of industrial applications involving heterogeneous reactions, such as pulverized coal combustion (PCC) or biomass gasification. To increase efficiency and decrease the environmental impact of new systems and optimize existing ones, more insight into the details of combustion processes is essential. Since combustion processes are a complex interaction of physical and chemical effects such as mass, momentum, heat and species transfer over a wide range of scales, also in conjunction with chemical reactions, even a simplified case description is complex. This restricts simulations of industrial scale combustion systems to be very coarse and use empirical models. This is especially true if a lot of cases have to be simulated for a parametric study.

A common approach used in industry and research is the Reynolds-Averaged Navier Stokes (RANS) model [1]. In addition, the first Large-eddy simulations (LES) are now employed for pilot scale systems [2]. These modelling approaches require subgrid models that account for flow and chemistry effects on scales that are smaller than what is resolved by the simulation. The subgrid models used in RANS and LES are developed by studying lab scale systems or numerical experiments using Direct Numerical Simulation (DNS), where all relevant turbulent scales are resolved. Although they are computationally expensive [3], DNS provide a way to non-intrusively study turbulent combustion systems and yield flow statistics that are difficult or impossible to obtain in real experiments [4]. This accurate description of the flow in DNS makes it especially suitable to study turbulent flows in detail. The insights gained can then be utilized to develop models and correlations that can be used in simulations of industrial systems.

It is known that turbulence affects combustion systems on different scales, from the recirculation zone behind a bluff body burner to small vortices in the flow far downstream. Turbulence is also essential for mixing and transport of physical properties, such as energy and species composition, which in turn have an influence on the reaction rates. For the case of homogeneous combustion, the interaction between turbulence and combustion has been studied extensively, and consequently a large variety of models have been developed. The review paper by Veynante and Vervisch [5] and the book by Poinso and Veynante [6] provide an excellent overview over the progress of homogeneous combustion research and the models for turbulence chemistry interaction that have been developed. For premixed flames e.g., models that are based on the interaction of scales [7], probabilities to find either burned or unburned gases [8, 9], or geometrical descriptions of

the flame [10, 11] can be used. In the case of non premixed flames with infinitely fast chemistry, one can use a presumed Probability Density Function (PDF) [12] or the Eddy Dissipation Concept (EDM), where the reactions are limited by either a deficiency of fuel, oxidizer or energy [13], or the Conditional Moment Closure (CMC), where all variable parameters are conditionally averaged on flow parameters such as the mixture fraction [14, 15]. If the chemistry is not assumed to be infinitely fast, the reaction rates may be obtained from flamelet libraries based on presumed PDFs of laminar flames or the shape of the flame [16]. Each of these models have individual strengths and shortcomings making them applicable to different combustion conditions.

Combustion of solid matter adds more complexity to the phenomena of turbulence chemistry interaction due to the multi phase nature of the problem. Depending on the composition of the fuel, each particle has to undergo drying, devolatilization/pyrolysis and finally heterogeneous combustion, all of which have to be accounted for in a complete description of the combustion process [17]. The interested reader is referred to the article of Eaton et al. [18] for a review on models used in pulverized coal combustion. However, to the authors' knowledge, there is no turbulence-chemistry model connecting the effect of turbulence to the process of conversion of a dried, devolatilized char particle, which is the objective of the present work.

A reacting particle and the surrounding turbulent flow are interacting on different scales, and these effects can increase or decrease the reaction rate depending on turbulence intensity. At the scale of a particle, the flow around the particle is responsible for transporting reaction products away from the particle surface, and bringing reactants to it. Additionally, turbulence increases heat transfer from and to the particle, leading to a change in the speed of reaction [19]. On larger scales, turbulence leads to a preferential concentration of particles [20, 21], where particles form dense particle clusters, separated by voids where nearly no particles are present. This can separate the solid fuel from the gaseous oxidizer. Describing the shape and size of these particle clusters and voids is a major research field in itself [22].

Annamalai and Ramalingam [23] performed a theoretical study of the combustion behaviour of clusters of coal particles in a quiescent flow and identify three distinct regimes, which are defined by low, medium or high particle concentrations inside the clusters. The Individual Particle Combustion (IPC) regime, is characterised by that the distances between particles are so high that their interaction can be neglected. For medium particle concentrations, the particles on

the outside of the clusters consume the oxidizer fast enough so that particles on the inside of the cluster react under fuel-richer conditions, which is called Group Combustion (GC). Finally, for high particle concentrations, the outermost shell of particles consumes all the oxidizer which is transported to it, effectively preventing oxidizing species transport to the internal particles. This combustion regime is called Sheath Combustion (SC), as only the sheath of the particle cluster is reacting. These regimes were found to have different combustion rates [23]. It is reported that in the IPC, a decrease in particle size (by particle break up, leading to an increase in particle number) results in an increase in the surface specific burning rate. In the SC regime, a decrease in particle size may result in a decrease of the surface specific burning rate. A similar finding is reported by Reveillon and Demoulin [24], who examined the evaporation behaviour of droplets in turbulent flows and found that the evaporation rate inside droplet clusters is slower than on the outside. This is due to the fast saturation of the fluid inside the droplet clusters and the slow mixing of saturated and unsaturated fluid.

Due to the increase of available computing power, DNS of pulverized coal jets under highly turbulent conditions have recently been published, providing insights into this complex phenomenon. Luo et al. performed a DNS of a pulverized coal jet flame [25] for a Reynolds number of around 30000 and compare their results qualitatively with experiments. They identify GC regimes at the jet nozzle and IPC regimes further downstream in the jet. A lab-scale pulverized coal jet flame was studied by Hara et al. [26], who propose a simple global reaction scheme that takes into account the effects of devolatilization products on the homogeneous reactions. A good agreement on the particle motion between simulation and experiments is reported. Moreover, they find different combustion regimes in the inner and outer flame layer. Brosh and Chackraborty investigated the effect of equivalence ratios and velocity fluctuations on pulverized coal combustion [27] and ignition [28] and found that the premixed combustion regime (which is more similar to IPC and GC than to SC) is more prominent for higher turbulent velocity fluctuations and vice versa. Moreover, an increase in velocity fluctuations is beneficial for mixing, but too high velocity fluctuations lead to flame extinction by increasing the heat transfer from the flame kernel. However, the published studies focus either on early stages of the combustion, where devolatilized fuel is the main driver of combustion [27], or on flows with non-isotropic turbulence [26]. While all studies account for char conversion, it is not explicitly studied.

The present work is part of an effort to provide a subgrid model to account for the effect of turbulence on heterogeneous reactions (such as char oxidation). DNS is used to study clustered char particles in a turbulent reacting flow and analyse

the effect of changing Damköhler numbers (from now on written as **Da**) on the char oxidation rates. It is an extension of earlier work that studied this effect in a simplified setup [29, 30], where the isothermal consumption of a passive scalar by particles in a turbulent flow was studied by DNS. This work is now extended to a DNS with heterogeneous reactions between reactive chemical species in order to study the interaction between the kinetics of heterogeneous reactions and turbulent clustering.

Although complex char oxidation reaction mechanisms exist [31, 32], the wide range of time scales of the individual reactions make a deduction of basic flow properties and timescales used in the analysis complicated. Moreover, calculating and storing many species and their reaction rates for both flow field and a large number of particles is prohibitively expensive, hence a simple mechanism is used in this work, although the mathematical framework is developed for a generic kinetic case.

The combustion process investigated in this work is represented by oxy-fuel combustion, which has been proposed as one measure to implement carbon capture technologies, and hence, decrease the environmental impact of fossil fuelled energy generation, as summarized in the review paper of Chen et al. [33]. The main difference between oxy-fuel and conventional combustion is that instead of air, pure oxygen together with recirculated flue gases, mainly CO<sub>2</sub>, is used as oxidizing agent. Thus it represents a simple case to study when only oxygen is assumed to be the oxidizing species.

The paper first gives an overview of the equations that are used to describe the fluid, the particles and their interaction in § 2, followed by an introduction of all dimensionless numbers in § 3. Thereafter, a model is proposed to describe the effect of turbulent clustering on the heterogeneous reaction rates, followed by the boundary and initial conditions of the DNS cases in § 4. In § 5, the data obtained is shown and compared with the proposed model, followed by a short discussion of the results and future work in Section § 6.

## **2. Numerical Modelling**

### *2.1. Fluid Equations*

For the DNS simulations shown in this work, "The Pencil-Code" [34] is used, which is an open source CFD code. It solves the fluid equations using a sixth-order finite difference scheme for spatial discretization and a compact third-order Runge-Kutta scheme [35] for temporal discretization. Gravity is neglected for both particle and fluid phase for simplicity and all domain boundaries are periodic.

The implementation of the homogeneous chemistry has previously been described in detail by Babkovskaia et al. [36]. The continuity equation is solved as

$$\frac{D\rho}{Dt} = -\rho\nabla \cdot \mathbf{u} + S_\rho, \quad (1)$$

where  $D/Dt = \partial/\partial t + \mathbf{u} \cdot \nabla$  is the advective derivative,  $\rho$  is the density,  $\mathbf{u}$  is the velocity and

$$S_\rho = \frac{-1}{V_{\text{cell}}} \sum_i^{N_{p,\text{cell}}} \frac{dm_{p,i}}{dt} \quad (2)$$

is the mass source term due to mass transfer from the particles to the fluid. In the above equation,  $m_{p,i}$  represents the mass of particle number  $i$ ,  $V_{\text{cell}}$  is the volume of the grid cell and the summation is over all particles  $i$  in the grid cell. The number of particles in the cell is given by  $N_{p,\text{cell}}$ . The momentum equation is written in the form

$$\rho \frac{D\mathbf{u}}{Dt} = -\nabla p + \nabla \cdot \boldsymbol{\tau} + \mathbf{f} + S_{m,p}, \quad (3)$$

where  $p$  is pressure and  $\mathbf{f}$  is a volume force. The volume force has random directions and wavelengths that are short compared to the length of the domain. The forcing mechanism is described in the work of Brandenburg et al. [37] and yields homogeneous isotropic turbulence. The viscous stress is given by:

$$\boldsymbol{\tau} = 2\rho\nu\mathbf{S}, \quad (4)$$

where  $\mathbf{S} = (1/2)(\partial u_i/\partial x_j + \partial u_j/\partial x_i) - (1/3)\delta_{ij}\nabla \cdot \mathbf{u}$  is the trace-less rate of strain tensor. Since the resolution in all cases is sufficient to resolve the smallest scales of the turbulence, no modelling of turbulence is required. The term  $S_{m,p} = (1/V_{\text{cell}}) \sum_i \dot{m}_{p,i}(\mathbf{u} - \mathbf{v}_{p,i})$  in Eq. (3) accounts for the momentum that is transferred to the fluid by the mass that is released from the particle with velocity  $\mathbf{v}_{p,i}$ . The equation for the mass fractions of each species is given by

$$\rho \frac{DY_k}{Dt} = -\nabla \cdot \mathbf{J}_k + \dot{\omega}_k + S_{y,k}, \quad (5)$$

where  $Y_k$  is the mass fraction of species  $k$ ,  $\mathbf{J}_k$  is the diffusive flux and  $\dot{\omega}_k$  is the chemical source term of species  $k$  due to homogeneous reactions, described in

detail in the work of Babkovskaia et al. [36], and

$$S_{y,k} = \frac{1}{V_{\text{cell}}} \sum_i^{N_{p,\text{cell}}} \left( \dot{W}_{k,i} + Y_k \frac{dm_{p,i}}{dt} \right) \quad (6)$$

is the source term due to gas phase species being involved in the heterogeneous reactions. Here,  $\dot{W}_{k,i}$  is the source of gas phase species  $k$  due to heterogeneous reactions on particle  $i$  (see Eq. (26)). The diffusive flux of species  $k$  is given by

$$\mathbf{J}_k = \rho Y_k \mathbf{V}_k \quad (7)$$

when  $\mathbf{V}_k$  is the diffusive velocity of species  $k$ . Finally, the energy equation is

$$\begin{aligned} c_v \frac{D \ln T_g}{Dt} = & \sum_k^{N_{\text{species}}} \left( -\nabla \cdot \mathbf{J} + \omega_k \right) \left( \frac{R}{m_k} - \frac{h_{s,k}}{T_g} \right) - \frac{R}{m_k} \nabla \cdot \mathbf{u} \\ & + \frac{2\nu \mathbf{S}^2}{T_g} - \frac{\nabla \cdot \mathbf{q}}{\rho T_g} + S_{T,\text{conv}} + S_{\text{enth}}, \end{aligned} \quad (8)$$

where  $T_g$  is the gas temperature,  $c_v$  is the heat capacity at constant volume,  $R$  is the universal gas constant,  $h_{s,k}$  is the sensible enthalpy of species  $k$ ,  $m_k$  is the molar mass of species  $k$ ,

$$\mathbf{q} = \sum_k^{N_{\text{species}}} h_k \mathbf{J}_k - k_g \nabla T_g \quad (9)$$

is the heat flux and  $h_k = h_{s,k} + \Delta h_{f,k}^0$  becomes the enthalpy of species  $k$  when  $\Delta h_{f,k}^0$  is the heat of formation of species  $k$ . The thermal conductivity is given by  $k_g$ . In the above equation, the sum of the conductive and convective heat transfer from the particles to the gas is given by

$$S_{T,\text{conv}} = \frac{1}{\rho T_g} \frac{1}{V_{\text{cell}}} \sum_i^{N_{p,\text{cell}}} Q_{c,i}, \quad (10)$$

when

$$Q_{c,i} = H_i A_{p,i} (T_{p,i} - T_g), \quad (11)$$

and the temperature of particle  $i$  is  $T_{p,i}$ . The mass that is transferred to the fluid carries enthalpy with it, which is accounted for by the term

$$S_{enth} = \frac{1}{\rho T_{gas}} \frac{1}{V_{cell}} \sum_i^{N_{p,cell}} \dot{W}_{k,i} h_{k,i}(T_{phase}). \quad (12)$$

The temperature  $T_{phase}$ , at which the species enthalpy is evaluated is taken from the phase where the species originated. When gas phase species are consumed, the enthalpy is evaluated at the gas phase temperature, if the species in question is produced by the particle, its enthalpy is evaluated at the particle temperature. The heat transfer coefficient  $H_i$ , taken from [38], can be expressed as

$$H_i = \frac{\text{Nu}_i k_g}{2r_{p,i}} \frac{B_i}{\exp(B_i) - 1} \quad (13)$$

when  $\text{Nu}_i$  is the Nusselt number obtained from the Ranz-Marshall [19] correlation:

$$\text{Nu}_i = 2 + 0.6 \text{Re}_{p,i}^{0.5} \text{Pr}^{0.33} \quad (14)$$

with  $\text{Pr}$  being the Prandtl number of the fluid, calculated as

$$\text{Pr} = \frac{\mu c_p}{k_g}, \quad (15)$$

where  $\mu$  is the dynamic viscosity of the fluid and  $c_p$  the heat capacity at constant pressure. The particle Reynolds number is given by

$$\text{Re}_{p,i} = \frac{d_{p,i} |\mathbf{v}_{p,i} - \mathbf{u}|}{\nu}, \quad (16)$$

when  $d_{p,i} = 2r_{p,i}$  is the particle diameter,  $r_{p,i}$  is the particle radius and  $A_{p,i} = \pi r_{p,i}^2$  is the cross sectional area of the particle. The Stefan flow constant in Eq. (13) is given by

$$B_i = \frac{\dot{m}_{p,i} c_v}{2\pi r_{p,i} \text{Nu}_i k_g}. \quad (17)$$



In this work, we use the ideal gas equation of state, such that the pressure is found as

$$p = \frac{\rho RT}{m}. \quad (18)$$

Detailed expressions for viscosity, species diffusion, thermal conduction, enthalpy and heat capacity are found in [36].

To increase the numerical stability of the simulations, the particle related source terms in the fluid equations  $S_\rho$ ,  $S_{Y,k}$ ,  $S_{m,p}$ , and  $S_{enth}$  are stored in temporary scalar or vector fields and diffused by Laplacian diffusion before being added to the fluid cells. A general flow variable  $\theta_0$  is stored in a scalar field before the diffusion steps. The value of the variable is then, after the  $n$ 'th diffusion step:

$$\theta_{n+1} = \theta_n + \frac{D_{num}\Delta t}{N_{step}}\nabla^2\theta_n, \quad (19)$$

when  $D_{num}$  is a numerical diffusion coefficient,  $\Delta t$  is the simulation timestep and  $N_{step}$  is the total number of diffusion steps per timestep. A compact 6-th order scheme is used to obtain the second derivative. The diffusion coefficient  $D_{num}$  is chosen as small as possible while ensuring stable calculations with three diffusion steps for every timestep. Of the total mass, energy or species transfer from a particle to the fluid, 80% is added to nodes directly neighbouring the node the particle is closest to. This approach greatly stabilizes the simulations without significantly changing the dynamics of the flow. An alternative to the approach described above is to use a spatial filter to distribute the effect of a particle onto several fluid grid points. The spatial filter would typically be a weighted distribution over the fluid grid points in the neighbourhood of the particle. For more numerical stability, a spatial filter with a larger radius of influence will be needed, which means that the effect of the particle will be distributed over more grid points. The effect of the radius of influence in such methods is studied by Sundaram and Collins [39]. During the development of the method used in the current work, comparisons with established interpolation methods for particle-fluid transfers, like the particle-in-cell-method (PIC) of Squires and Eaton [40] and the projection onto neighbouring nodes (PNN) method as used by Elghobashi and Truesdell [41], have been performed. The method used in this work (Eq. (19)) yielded results that lie between the PIC and the PNN.

## 2.2. The particle equations

The particle model of the Pencil-Code has been extended to account for reactive particles, which exchange momentum, mass, species and energy with the fluid. A detailed description of the particle reaction model can be found in Haugen et al. [38, 42]. The only momentum transfer from the particles to the fluid is via the mass they transfer to the fluid. The back reaction due to the particle drag force is not considered in this work, since its focus lies not on turbulence statistics. The particles are regarded as point particles, displacing no fluid, which is valid for particles that are much smaller than the grid cells. Furthermore, particle-particle interactions are not considered due to the dilute nature of the flow. Particle tracking is achieved using a Lagrangian formalism where the evolution equation for the particle velocity is given as

$$\frac{d\mathbf{v}_p}{dt} = \frac{\mathbf{F}_p}{m_p}, \quad (20)$$

and for the position as

$$\frac{d\mathbf{x}}{dt} = \mathbf{v}_p, \quad (21)$$

where  $m_p$ ,  $\mathbf{v}_p$  and  $\mathbf{x}$  are the mass, velocity and position of the particle's centre of mass, respectively. Furthermore, the force  $\mathbf{F}_p$  is the sum of all forces acting on the particle. Since gravity is neglected, and since a high density ratio between the particles and the fluid is assumed, the only force on the particles that has to be considered is the drag force. The Stokes drag, with extension to low and medium particle Reynolds numbers, is used in the present work. This means that the total force acting on the particles is given by

$$\mathbf{F}_p = \frac{1}{2}\rho C_D A_p |\mathbf{u} - \mathbf{v}_p| (\mathbf{u} - \mathbf{v}_p) = \frac{m_p}{\tau_p} (\mathbf{u} - \mathbf{v}_p), \quad (22)$$

when

$$\tau_p = \frac{2m_p}{\rho C_D \pi r_p^2 |\mathbf{u} - \mathbf{v}_p|} = \frac{8\rho_p r_p}{3\rho C_D |\mathbf{u} - \mathbf{v}_p|} = \frac{S d_p^2}{18\nu(1 + f_c)} \quad (23)$$

is the particle response time (Stokes time). In this equation,  $S = \rho_p/\rho$  is the density ratio between a particle and the fluid. The extended Stokes drag coefficient

is

$$C_D = \frac{24}{\text{Re}_p}(1 + f_c), \quad (24)$$

where  $f_c = 0.15\text{Re}_p^{0.687}$  is due to the Schiller-Naumann correlation, which is valid for particle Reynolds numbers up to 800 [43]. The particles in our simulations have a mean particle Reynolds number of 0.1. The mass loss rate of a single particle is calculated as:

$$\frac{dm_p}{dt} = - \sum_k^{N_{\text{species}}} \dot{W}_k, \quad (25)$$

while the net species mass production rate is given by

$$\dot{W}_k = A_p \widehat{RR}_k M_k. \quad (26)$$

The surface area of the particle is denoted  $A_p$ , the molar mass of species  $k$  is  $M_k$  and

$$\widehat{RR}_k = \sum_j^{N_{\text{reactions,het}}} (v''_{j,k} - v'_{j,k}) \widehat{R}_j \quad (27)$$

is the surface specific molar production rate of species  $k$ . The stoichiometric coefficients  $v'_{j,k}$  and  $v''_{j,k}$  are for the reactant and product side of reaction  $j$ , respectively. The rate of reaction  $j$  is given by:

$$\widehat{R}_j = k_{\text{kin},j} \left( \prod_l^{N_{\text{species}}} (X_{l,s} C_g)^{v'_{j,l}} \right). \quad (28)$$

Here,  $X_{l,s}$  is the mole-fraction of species  $l$  at the particle surface,  $C_g$  is the local gas concentration, which is evaluated at the particle film temperature  $T_{\text{film}} = T_p + (T_g - T_p)/3$  and found from the ideal gas law;

$$C_g = \frac{N_m}{V} = \frac{P}{RT_{\text{film}}}. \quad (29)$$

In this equation,  $N_m$  represents the number of moles in the volume  $V$ . The kinetic rate of reaction  $j$  is given by the Arrhenius expression

$$k_{kin,j} = B_{n,j} T^{\alpha_{n,j}} \exp(-E_{an,j}/RT_p), \quad (30)$$

where  $B_n$  is the pre-exponential factor,  $\alpha_n$  is the temperature exponent, and  $E_{an}$  the activation energy, which are all empirical coefficients that are given by the kinetic mechanism.

For a single irreversible global heterogeneous reaction with only one homogeneous reactant species  $r$ , an algebraic solution for the surface mole fraction  $X_{r,s}$  of the reactant can be found by applying the Baum and Street model [44] and assuming equilibrium between the transport and consumption of the reactant  $r$ :

$$\underbrace{X_{r,s} \dot{n}_{total}}_{Stefan\ Flow} - \underbrace{C_g k_{diff} (X_{r,\infty} - X_{r,s})}_{Diffusion} = \underbrace{C_g k_{kin} X_{r,s}}_{Production/Consumption}. \quad (31)$$

If the heterogeneous reaction is unimolar, i.e.  $\dot{n}_{total} = 0$ , Eq. (31) gives a very simple expression for the mole fraction of reactant  $r$  at the particle surface;

$$X_{r,s} = \frac{X_{r,\infty} k_{diff}}{k_{kin} + k_{diff}}, \quad (32)$$

when  $k_{diff}$  is the mass transfer coefficient. For multiple reactant species, a multi-variate set of Eq. (32) can be solved by a Newton-Raphson method. As long as the particle is much smaller than the fluid grid cell, the expression in Eq. (32) makes it possible to use the mean reactant mole fraction in the grid cell,  $X_{r,\infty}$ , instead of the reactant mole fraction at the particle surface,  $X_{r,s}$ . For a single reaction with one reactant species, Eq. (28) then reduces to

$$\widehat{R} = k_{eff} X_{r,\infty} C_g, \quad (33)$$

when the mean effective reaction coefficient,

$$k_{eff} = \frac{k_{kin} k_{diff}}{k_{kin} + k_{diff}}, \quad (34)$$

is introduced to account for kinetic reaction rate as well as diffusive transport of reactant to the particle. The term  $k_{diff}$  is the mass transfer rate, which is defined

by

$$k_{diff} = \frac{DSh}{2r_p}, \quad (35)$$

where  $D$  is the diffusivity in the bulk gas and

$$Sh = 2 + 0.69Re_p^{0.5} Sc^{0.33} \quad (36)$$

is the particle Sherwood number, which is obtained using the Ranz-Marshall correlation [19] for flows with low and intermediate Reynolds numbers. Here,  $Re_p$  is the particle Reynolds number and  $Sc$  the Schmidt number. It is interesting to note that for a RANS simulation, the relative velocity between the particles and the fluid is not available since the turbulence velocity is not resolved. In many RANS modelling tools, it is therefore customary to include some kind of particle dispersion model, where the particles are displaced in random directions and distances based on the local turbulence parameters in order to make the particles diffuse through the fluid. As a by-product of the particle dispersion that is obtained with these models, there will be a relative velocity between the particles and the fluid, but, since no account is made for the correlation with the instantaneous turbulent structures, this velocity does not have anything to do with the reality. It is therefore often better to simply neglect the effect of the relative particle-fluid velocity by setting the particle Reynolds number in Eq. (36) to zero, such that the Sherwood number becomes 2. Hence, for a quiescent fluid, or for a RANS simulation, the Sherwood number is 2 and the mass transfer coefficient then reduces to

$$k_{diff,q} = D/r_p. \quad (37)$$

The particle temperature evolution is given by:

$$\frac{dT_p}{dt} = \frac{1}{m_p c_{p,p}} (Q_{reac} - Q_c + Q_{rad}), \quad (38)$$

where  $Q_{reac}$  is the heat due to the surface reactions,  $Q_c$  the conductive heat loss to the fluid and  $Q_{rad} = 4\epsilon\sigma\pi r_p^2(T_s^4 - T_p^4)$  is the radiative heating of the particle. Here,  $\epsilon$  is the emissivity,  $\sigma$  the Stefan-Boltzmann constant and  $T_s$  is the temperature of the surroundings. If  $T_p > T_s$ , this corresponds to a situation where the particles are radiatively cooled, acting as heat sinks in the system. The particle heat capacity is denoted by  $c_{p,p}$ . The particle is assumed to be thermally thin, resulting in a

uniform temperature distribution throughout the particle.

The reactive heating rate is given by:

$$Q_{\text{reac}} = A_{p,i} \sum_j^{n_{\text{reactions}}} \widehat{R}_j h_j, \quad (39)$$

when the heating due to reaction  $j$  is composed of the surface specific reaction rate  $\widehat{R}_j$  and the heat of reaction  $h_j$ . The specific enthalpies are calculated at the particle temperature for all products and for all solid reactants, and at the gas temperature for gaseous reactants. The reactive heating only heats up the particle, as the heat loss to the fluid is already accounted for by evaluating the species enthalpy that is transferred to the fluid at the particles temperature in the term  $S_{\text{enth}}$  in Eq. (12).

### 3. Dimensionless numbers

In this work, four dimensionless numbers are of special interest and therefore explained in detail: The Damköhler number  $Da$ , the Sherwood number  $Sh$ , the particle Stokes number  $St$  and the Sherwood correction factor  $\tilde{\alpha}$ . The Damköhler number is the ratio between the turbulent time scale  $\tau_L$  and the chemical time scale  $\tau_{\text{hom}}$ :

$$Da = \frac{\tau_L}{\tau_{\text{hom}}}, \quad (40)$$

where  $\tau_{\text{hom}}$  is the inverse of the ideal homogeneous reaction rate. If we assume a reactive object, which is typically a particle or a dense cluster of particles, the ideal homogeneous reaction rate then depends on the mean reactive surface area of the object  $\overline{A}'$ , the mean reactive density  $\overline{n}'$  and its effective reaction rate  $\overline{k}'_{\text{eff}}$ . Accordingly,  $\tau_{\text{hom}}$  can be expressed as

$$\tau_{\text{hom}} = \frac{1}{\alpha_{\text{hom}}} = \frac{1}{\overline{A}' \overline{n}' \overline{k}'_{\text{eff}}}, \quad (41)$$

such that the Damköhler number becomes:

$$Da = \alpha_{\text{hom}} \tau_L = \overline{A}' \overline{n}' \overline{k}'_{\text{eff}} \tau_L. \quad (42)$$

The turbulent time scale considered in this work is the time scale  $\tau_L$  of the integral scale,  $l = L/2\pi k_f$ , which is given by

$$\tau_L = \frac{L}{2\pi k_f u_{\text{RMS}}}, \quad (43)$$

where  $L$  is the domain size,  $k_f$  is the wave number of the external forcing and the root mean square velocity is  $u_{\text{RMS}}$ .

The particle Stokes number is given by the ratio between the particle response time and the turbulent time scale:

$$\text{St} = \frac{\tau_p}{\tau_L}. \quad (44)$$

To achieve clustering at the large scales of the flow, the density and radius of the particles are chosen so that for the simulations in this work a Stokes number of approximately 1 is achieved.

### 3.1. The ideal homogeneous reaction rate and the Damköhler number

For low  $\text{Da}$ , the fluid composition and temperature is relatively homogeneously distributed throughout the domain. This means that the fluid surroundings of a given particle is not directly influenced by the particles in its immediate neighbourhood, but rather by the accumulated effect of all particles in the domain. Thus, the reaction rate, and hence also the Damköhler number, scale proportionally to the mean surface area of the particles  $\bar{A}' = \bar{A}_p$ , the mean particle number density in the domain  $\bar{n}' = \bar{n}_p$  and mean effective particle reaction rate  $\bar{k}'_{eff} = \bar{k}_{eff,p}$ , which means that the Damköhler is given by

$$\text{Da} = \bar{A}_p \bar{n}_p \bar{k}_{eff,p} \tau_L = \alpha_{hom,q} \tau_L, \quad (45)$$

when the ideal homogeneous reaction rate is

$$\alpha_{hom,q} = \bar{A}_p \bar{n}_p \bar{k}_{eff,p}, \quad (46)$$

for a quiescent fluid ( $\text{Sh}=2$ ) and a mean effective particle reaction rate  $\bar{k}_{eff,p}$  that is equal to the mass transfer rate  $k_{diff}$ , is established as a base value to compare against. This case, when  $k_{diff} = k_{eff,p}$ , corresponds to the situation when  $k_{diff} \ll k_{kin}$ , i.e., when the reactions are diffusion controlled. The ideal homogeneous reaction rate is also used to define the Damköhler number of each case.

### 3.2. Low Damköhler number in turbulence

For low  $\mathbf{Da}$  and diffusion limited reaction rates, the actual reaction rate is higher than the ideal homogeneous reaction rate. This is due to the fact that the ideal homogeneous reaction rate (Eq. (46)) is based on a quiescent flow, for which the Sherwood number is 2 according to the Ranz-Marshall correlation [19]. The actual Sherwood number is higher than 2 because of the relative motion of particle and fluid. The increase in the reaction rate becomes the ratio of the actual Sherwood number divided by two. When account is made for the relative fluid-particle velocity due to turbulence, the mean effective diffusion limited particle reaction rate is therefore given by:

$$\underbrace{\alpha_{hom,t}}_{turbulent} = \alpha_{hom,q} \frac{Sh}{2}. \quad (47)$$

Note that in this regime, the reaction rate still scales linearly with the number density of particles,  $\bar{n}_p$ .

### 3.3. High Damköhler number, SC regime

It is known that particles embedded in a turbulent flow will form particle clusters where the particle number density is significantly above the mean value [20, 21, 22]. For large  $\mathbf{Da}$ , the particle number density inside these clusters is very high and the internal oxygen is consumed rapidly. Following the description in the work of Haugen et al. [30], the characteristic length scale  $l$  of these particle clusters is obtained by assuming that the eddies responsible for the clustering have the same time scale as the clustering particles, such that  $\tau_l = \tau_p = St\tau_L$ . Assuming Kolmogorov scaling between the scales  $l$  and  $L$ , one obtains  $l = LSt^{3/2}$  and  $D_{diff,cl} = u_l l = u_{RMS} LSt^2$  [30]. The subscript  $cl$  stands for all cluster related properties. After the internal oxygen is consumed, the reaction rate is limited by the transport of oxygen to the surface of the particle clusters. This is a combustion regime similar to Sheath Combustion [23], and the reaction rate converges to a *particle number density independent* value  $\alpha_{cl}$  [30]:

$$\alpha_{cl} = \bar{A}_{cl} \bar{n}_{cl} \bar{k}_{diff,cl} = A_1 A_2 \frac{D_{diff,cl} Sh}{l^2}. \quad (48)$$

The cluster dependent reaction rate,  $\alpha_{cl}$ , is dependent on the mean cluster surface area  $\bar{A}_{cl} = A_1 l^2$ , the mean cluster number density  $\bar{n}_{cl} = A_2 / l^3$  and the cluster dependent mass transfer rate  $\bar{k}_{diff,cl} = D_{diff,cl} Sh / l$ , where  $A_1$  and  $A_2$  are fitting



factors related to the shape of the particle clusters, influencing their number and surface area, respectively. Inserting the expressions for  $l$  and  $D_{diff,cl}$  into Eq. (48) then yields:

$$\alpha_{cl} = \frac{A_1 A_2 \text{Sh}}{\tau_L \text{St}}. \quad (49)$$

Haugen et al. [30] determined values for  $A_1 A_2$  for a range of  $\text{Re}_L$  and  $\text{St}$  and they arrive at the following functional dependence;  $A_1 A_2 = 0.08 + \text{St}/3$ , which predicts the effect of turbulent clustering on the reaction rate in a simpler system. Note that the expression for  $\alpha_{cl}$  has no dependence on the number of individual particles.

### 3.3.1. Connecting IPC and SC combustion regimes

A model for the reaction rate connecting the limits for small and large  $\text{Da}$  (IPC and SC in the terminology of Annamalai and Ramalingam) can be obtained by constructing the harmonic mean:

$$\alpha = \frac{\alpha_{cl} \alpha_{hom,t}}{\alpha_{cl} + \alpha_{hom,t}}. \quad (50)$$

By dividing this expression by the ideal homogeneous reaction rate for a quiescent fluid, a Sherwood correction factor  $\tilde{\alpha} = \alpha / \alpha_{hom,q}$  can be found as:

$$\tilde{\alpha} = \frac{\alpha_{cl}}{\alpha_{cl} + \text{DaSh}/(2\tau_L)} \frac{\text{Sh}}{2}. \quad (51)$$

This expression takes into account both the influence of the turbulence on each individual particle via the Sherwood number, as well as the influence of large scale clustering via the cluster dependent reaction rate  $\alpha_{cl}$ .

If the chemical timescale, the turbulent flow time scale and the particle Stokes number are known properties the Sherwood correction factor can be obtained and combined with Eq. (37) to obtain a mass transfer rate

$$k_{diff,turb} = \tilde{\alpha} k_{diff,q} \quad (52)$$

that takes into account the effect of small scale turbulence and turbulent clustering.

### 3.4. Finding the Sherwood correction factor from simulations

To validate the model in Eq. (51), we compare the mean mass loss rates of the particles obtained from the DNS simulations with the mean homogeneous

mass loss rate of the same case. In current state of the art RANS models for char conversion, no model exists that accounts for the effect of turbulence on the heterogeneous reactions. The mean homogeneous mass loss rate, which is the mass loss rate one would obtain if small char particles were homogeneously mixed in a quiescent fluid, is therefore what is used in a typical RANS simulation. The aim of this paper is to provide a model for heterogeneous combustion of char that accounts for the effects of turbulence and that can be used for any RANS simulation.

Based on Eq. (34), the mean effective reaction coefficient in a quiescent fluid is given by

$$k_{eff,q} = \frac{k_{kin}k_{diff,q}}{k_{kin} + k_{diff,q}}, \quad (53)$$

when  $k_{diff,q}$  is found from Eq. (37). The mean homogeneous mass loss rate is found by combining Eq. (25) and Eq. (26), such that

$$\frac{d\bar{m}_{p,hom}}{dt} = -\bar{A}_p M_k \sum_k^{N_{species}} \bar{R}R_k. \quad (54)$$

For a single reaction with only one reactant, where the reaction removes one carbon atom from the surface of the char particle, Eqs. (53) and (54) can then be combined with Eqs. (27) and (33) to yield

$$\frac{d\bar{m}_{p,hom}}{dt} = -\bar{A}_p M_c \bar{k}_{eff,q} \bar{X}_{r,\infty} \bar{C}_g. \quad (55)$$

As argued in § 3.3.1, the turbulence only affects the mass transfer rate to the particles, not the kinetic rate. The corresponding mean effective reaction coefficient that incorporates the effect of turbulence is therefore given by

$$k_{eff,turb} = \frac{k_{kin}k_{diff,turb}}{k_{kin} + k_{diff,turb}}, \quad (56)$$

when  $k_{diff,turb}$  is found from Eq. (52). Hence, the actual mass loss rate in a turbulent flow is given by

$$\frac{d\bar{m}_p}{dt} = -\bar{A}_p M_c \bar{k}_{eff,turb} \bar{X}_{r,\infty} \bar{C}_g. \quad (57)$$

By combining Eqs. (55) and (57), the ratio of the mean *actual* mass loss rate,

which includes the effect of turbulence, to the mean homogeneous mass loss rate, which neglects the effect of turbulence, is found to be

$$\beta = \frac{d\bar{m}_p/dt}{d\bar{m}_{p,hom}/dt} = \frac{k_{eff,turb}}{k_{eff,hom}}. \quad (58)$$

This is a measure of how fast the reactions proceed compared to the homogeneous assumption. From Eqs. (53) and (56), it can then shown that

$$\beta = \frac{k_{kin}\tilde{\alpha}k_{diff,q}/(k_{kin} + \tilde{\alpha}k_{diff,q})}{k_{kin}k_{diff,q}/(k_{kin} + k_{diff,q})} = \frac{\tilde{\alpha}(k_{kin} + k_{diff,q})}{k_{kin} + \tilde{\alpha}k_{diff,q}}. \quad (59)$$

Solving for the Sherwood correction factor,  $\tilde{\alpha}$ , yields:

$$\tilde{\alpha} = \frac{\beta k_{kin}}{k_{kin} + k_{diff,q}(1 - \beta)}. \quad (60)$$

This expression takes into account the effect of the ratio between the kinetic and the diffusive rate on the Sherwood correction factor. When  $k_{kin} \gg k_{diff}$ ,  $\tilde{\alpha}$  is nearly proportional to  $\beta$ . However, when the reaction is kinetically controlled,  $\tilde{\alpha}$  is less dependent on  $\beta$ . In short, a Sherwood correction factor of 1 describes no change in the reaction rates in comparison to the homogeneous assumption *in a quiescent fluid*, a ratio  $\tilde{\alpha} > 1$  signifies a speed-up, and a value  $\tilde{\alpha} < 1$  corresponds to a slow-down.

In § 5, the value of  $d\bar{m}_p/dt$  is given by the actual mass loss rate obtained from the DNS simulation, while  $d\bar{m}_{p,hom}/dt$  is found from Eq. (55). The Sherwood correction factor is then determined from Eq. (60).

#### 4. Simulation setup

For simplicity, char is here considered to react with oxygen to form carbon dioxide. Hence, no homogeneous reactions are present, and the gas phase source term,  $\dot{\omega}_k$  in Eq. (5), is zero. The heterogeneous mechanism is taken from the work of Li and You [45] and summarized in table 1. To achieve relatively constant Stokes and **Da** for the duration of the simulation, the particles react with oxygen present in the fluid and transfer mass to the fluid phase while the particles themselves do not lose mass. This allows us to exclude the effects of varying Damköhler and Stokes numbers, and therefore different clustering or mass transfer behaviour, from the present analysis. The reactions assume a fully dried and

Table 1: Heterogeneous mechanism

| $C + O_2 \rightarrow CO_2$ |               |                  |
|----------------------------|---------------|------------------|
| $B_n[m/s]$                 | $\alpha_n[-]$ | $E_n[J/mol]$     |
| $1.2 \cdot 10^4$           | 0             | $101 \cdot 10^3$ |

devolatilized char particle reacting with oxygen in isotropic and homogeneous turbulence. This setup is ment to resemble what would be observed when studying a small fluid volume that is advected with the mean flow downstream of the zone of gas phase combustion. The Damköhler number is varied from simulation to simulation by varying the number of particles in the domain according to Eq. (45).

#### 4.1. Initialization and start time of reactions

All cases are initialized with random particle positions and then run with reactions disabled until a statistically steady state is reached, which is determined by a stabilization of the shape of the PDF of the particle number density. The evolution of the PDF of the particle number density over time is presented in Fig. (1). As can be seen, the initial distribution is close to a gaussian distribution, which is expected from a true random distribution. As the simulation progresses, the PDF broadens to show a high number of cells with few particles, but also a significant number of cells with many particles. This corresponds to clusters of particles, separated by voids with nearly no particles present. The mean relative velocity between the particles and the fluid varies around a constant value, as shown in Fig. (2) for a representative case. A simulation time of 0.06 seconds, which corresponds to 16 eddy turnover times, is sufficient to reach a statistically steady state for all cases. The long term variation in relative particle velocity that occur after the reactions are turned on is due to the effect of chemical reactions on temperature and fluid composition. Only data from when the mean oxygen mass fraction is still above 1% is taken into account in the subsequent analysis.

#### 4.2. Particle size to grid size dependence

Attention must be given to the fact that the ratio of the particle diameter to the square of the cell size should not exceed a certain value. If a single particle in a cell represents too much reactive surface, the cell's oxygen content is rapidly consumed and a region devoid of oxygen forms around the particle. In the work of Annamalai and Ramalingam [23], this zone is called the film zone and the particle is undergoing Individual Particle Combustion. This is a physical effect, which

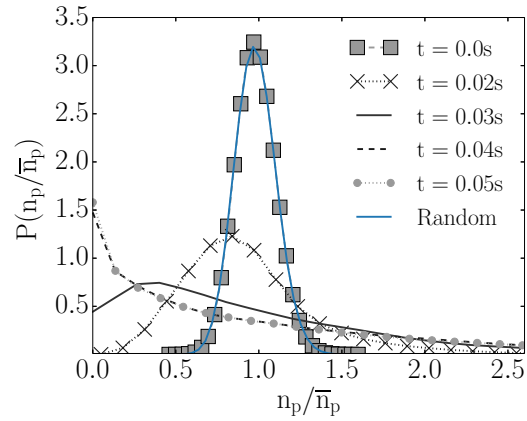


Figure 1: Evolution of the PDF of the particle number density over time

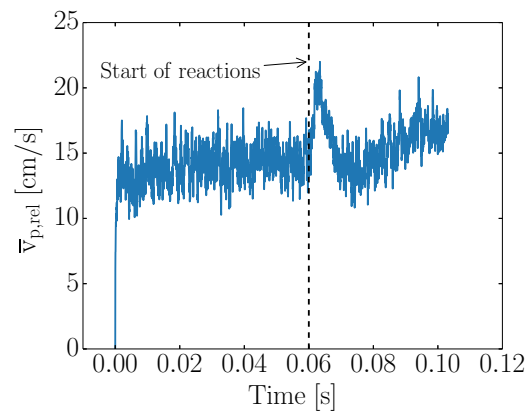


Figure 2: Evolution of the relative particle velocity over time.

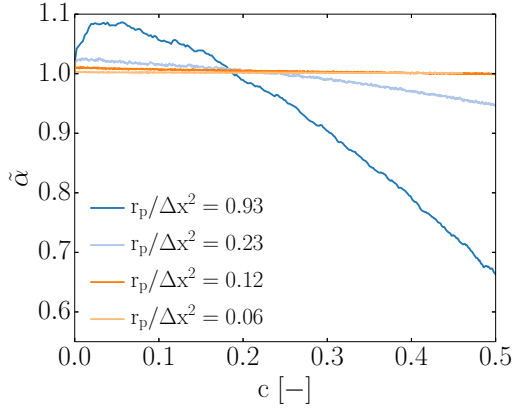


Figure 3: Ratio of the real to the ideal homogeneous reaction rate for a constant Damköhler number of 0.1 for different particle sizes as a function of oxygen conversion.

leads to a reaction rate that is lower than the ideal homogeneous reaction rate, even for small Damköhler numbers. In addition, particles that are large compared to the grid cell tend to introduce numerical instability in the simulations, and, in extreme cases, they will also violate the point-particle assumption that the particle tracking model is based upon. To mitigate these numerical issues, and the forming of a significant "film zone" around each particle, sufficiently small particles are needed. To hold the Damköhler number constant when decreasing the particle surface area, the number density  $n_p$  of particles has to be increased according to Eq. (41). This effect is illustrated in Fig. (3), where the Sherwood correction factor is shown to decrease for increasing oxygen conversion and larger ratios of  $r_p/\Delta x^2$ . The oxygen conversion is defined as:

$$c(t) = 1 - \frac{\bar{Y}_{O_2}(t)}{Y_{O_2,0}}. \quad (61)$$

Figure 4 shows the oxygen mass fraction for simulations with decreasing particle sizes and increasing particle numbers from left to right. All cases have the same low Damköhler number. The areas of low oxygen content around single, large particles are particularly visible in the leftmost panel. Moving towards the right panel it is clear that for smaller particles, the oxygen distribution is more uniform. When decreasing the particle size, the Damköhler number is kept constant by increasing the particle number density. For turbulent cases, it is also important to maintain the same Stokes number, which is achieved by increasing the material

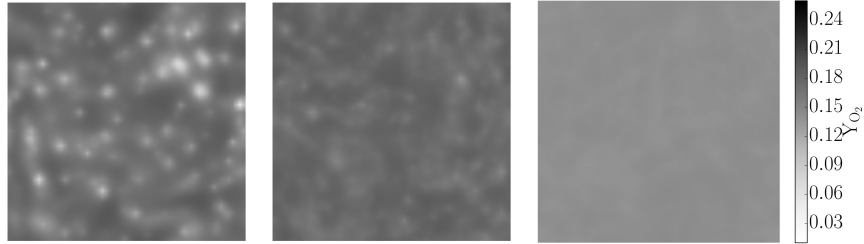


Figure 4: Plots of the oxygen mass fraction for cases with increasing particle numbers and decreasing particle radii at a low and constant Damköhler number.

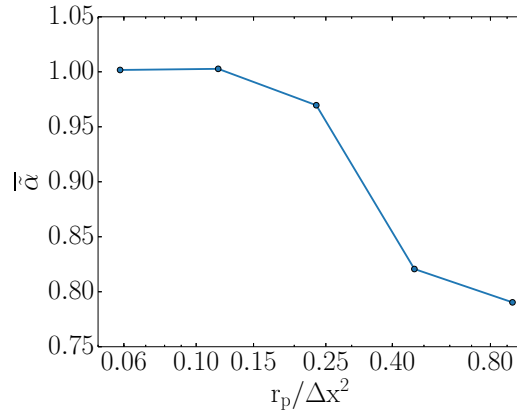


Figure 5: Ratio of the real to the ideal homogeneous reaction rate for a constant Damköhler number of 0.1 over the ratio  $r_p / \Delta x^2$ .

density of the particles.

The Sherwood correction factor is shown as a function of the particle size ( $r_p / \Delta x^2$ ) for  $Da = 0.1$  in Fig. (5). It can be seen from the figure that the Sherwood correction factor starts to decrease for  $r_p / \Delta x^2 > 0.12$ . This decrease is, as explained previously, due to the presence of a film zone with lower oxygen around the large particles. To avoid having to account for the effect of the film zone, a particle radius of  $11.25 \mu\text{m}$  ( $r_p / \Delta x^2 = 0.12$ ) is chosen for the remainder of the simulations. To satisfy the requirement of a Stokes number of unity, a large density ratio between particle and fluid is required. This would not be a requirement for larger Reynolds numbers though, since the flow time scale would be reduced. Table 2 summarizes the general conditions of all simulations.

Table 2: Common boundary conditions of the cases. Here, subscript 0 refers to the initial condition.

|               |  |
|---------------|--|
| $T_{gas,0}$   | 2100 [K]                               |
| $T_{wall,0}$  | 2100 [K]                               |
| $T_{p,0}$     | 2100 [K]                               |
| $\rho_{char}$ | 8.55 [g/cm <sup>3</sup> ]              |
| $\rho_{gas}$  | $3 \cdot 10^{-4}$ [g/cm <sup>3</sup> ] |
| $u_{RMS}$     | 180.0 [cm/s]                           |
| Re            | 40 [-]                                 |
| $L_f$         | 1/1.5 [cm <sup>-1</sup> ]              |
| $Y_{CO_2,0}$  | 0.74 [-]                               |
| $Y_{O_2,0}$   | 0.26 [-]                               |
| $L$           | 6.28 [cm]                              |
| $r_p$         | 11.25 [ $\mu$ m]                       |
| $N_{cell}$    | 64 <sup>3</sup> [-]                    |

## 5. Results

Figure 6 shows the Damköhler number as given by Eq. (42) as a function of oxygen conversion for cases with different particle number densities. Higher particle number densities yield higher **Da**, and the Damköhler number for each case increases until 75% conversion, and then decreases again. The change in fluid diffusivity with temperature is the most important fluid property influencing the variability of the Damköhler number.

Figure 7 shows the ratio of the kinetic to the mass transfer rate for cases with different **Da**, plotted as a function of oxygen conversion. The ratio first increases, with the maximum being higher for lower **Da**. The reason for this is that the amount of oxidizer per particle is higher for lower **Da**. This means that for low **Da**, the particles obtain higher temperatures, and hence larger values of  $k_{kin}$ . The decrease in the kinetic rate at later times is due to radiative particle cooling. It is clear from the figure that for these simulations, the char conversion is diffusion controlled for low Damköhler numbers.

### 5.1. The reaction rate, oxygen consumption and inhibition

The decrease of oxygen content over time can be seen in Fig. (8) for several **Da**. The x-axis is at 1%  $Y_{O_2}$ , which illustrates the large differences in time to reach this mass fraction. The case with the highest Damköhler number reaches 1% mass fraction of oxygen after 0.02s, while the case with the lowest Damköhler number



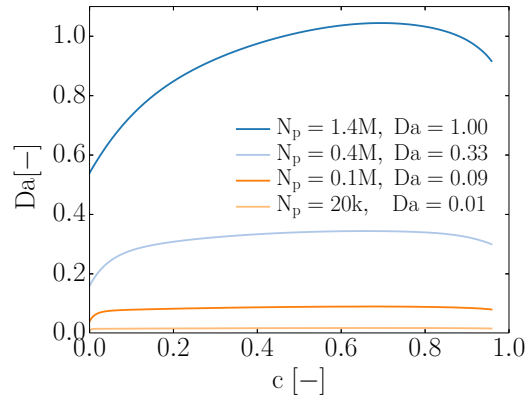


Figure 6: Evolution of the Damköhler number over time.

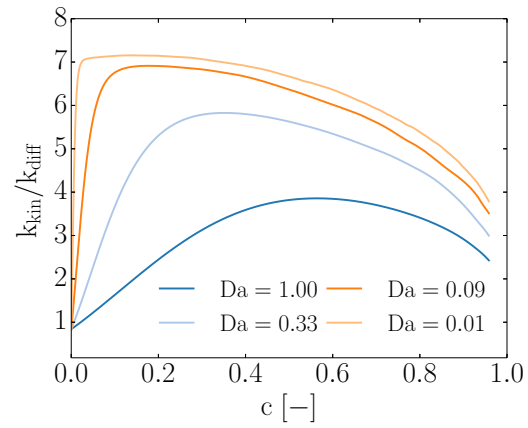


Figure 7: Ratio of kinetic and mass transfer rate over time.

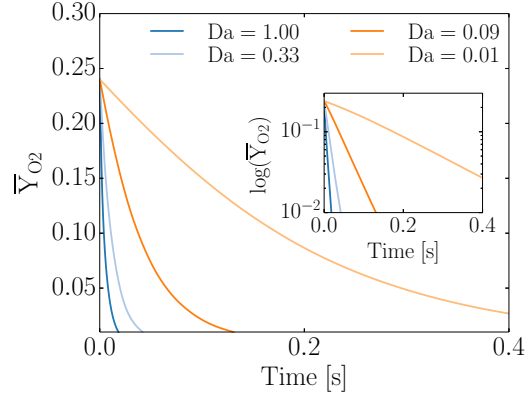


Figure 8: Evolution of the mean oxygen mass fraction over time.

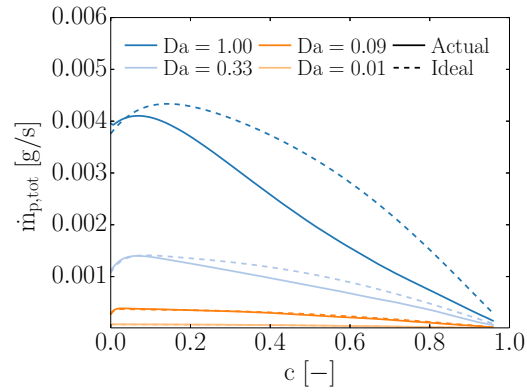


Figure 9: Comparison of ideal and actual total particle mass loss rates over time for simulations with different  $\mathbf{Da}$ .

takes 60 times longer, i.e. 1.2s. The mean oxygen mass fraction decreases near exponentially, which can be seen in the inset. The exponential decay is expected from a first order reaction equation [29]. In Fig. (9), the actual total particle mass loss rate ( $d\bar{m}_p/dt$ ) and the ideal homogeneous mass loss rate ( $d\bar{m}_{p,hom}/dt$ ), assuming homogeneous distribution of particles, are compared for several  $\mathbf{Da}$ . For low conversions (early times), all cases show comparable ideal and actual mass loss rates. For higher conversion values, the ideal mass loss is higher than the actual one, and the difference is stronger for higher  $\mathbf{Da}$ . The fastest reactions are found in the beginning, when oxygen is still available inside the particle clusters. The reason for the difference between the ideal and the actual mass loss for high  $\mathbf{Da}$  is that the particle clusters become void of oxygen, even though there are large

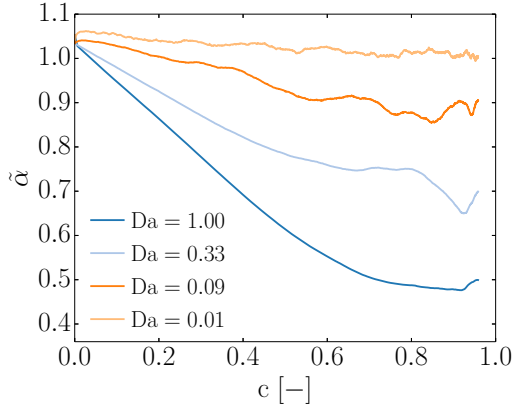


Figure 10: Sherwood correction factor over conversion for simulations with different Damköhler numbers.

amounts of oxygen available between the clusters. This means that the ideal homogeneous mass loss is only taking into account the total amount of oxygen in the domain or cell, while the actual mass loss is also taking into account the distribution of oxygen and particles. Figure 10 shows the corresponding Sherwood correction factor over conversion, as obtained from Eq. (60), for the same cases as was shown in Fig. (9). The curve ends when the mass fraction of oxygen has reached 1%. The decrease of the Sherwood correction factor for high  $Da$  is clearly seen. It can also be seen that the Sherwood correction factor has a tendency to decrease with conversion for conversions less than about 50%. The reason that the Sherwood correction factor is higher for early times is that the particles clusters are not yet void of oxygen. For larger conversions, a clear positive or negative trend in the behaviour of the Sherwood correction factor is no longer seen, and we therefore choose to define the steady state Sherwood correct factor as the value obtained in the range from 50%-99% conversion.

In Fig. (11), the steady state Sherwood correction factor is plotted over Damköhler number for a range of different simulations. The small scale influence of turbulence can be seen in the fact that for small  $Da$ , the reaction rate is faster than the ideal homogeneous one (i.e.  $\tilde{\alpha} > 1$ ). This is due to the fact that the turbulence induces a relative velocity between the particles and the fluid, which results in fresh reactants constantly being convected to the particle surface, and hence, that the conversion rate is increased.

For large Damköhler numbers ( $Da > 0.3$ ), the Sherwood correction factor is less than unity. This is due to the effect of the particle clustering, where the fluid in

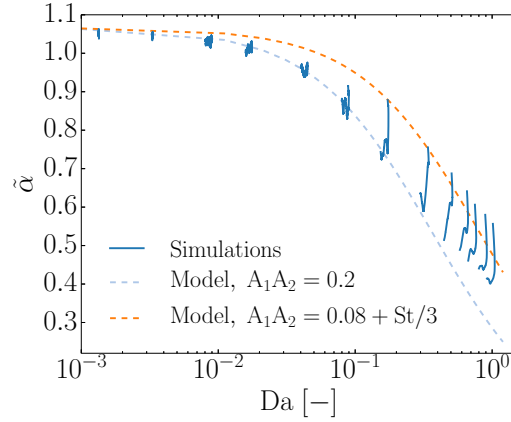


Figure 11: Sherwood correction factor over the Damköhler number

the particle clusters are depleted of oxygen, while there is still significant amounts of oxygen left in the volumes between the clusters. The dashed lines in Fig. (11) represent the model for the Sherwood correction factor, as given by Eq. (51), where the cluster dependent reaction rate,  $\alpha_{cl}$ , is given by Eq. (48). The Sherwood number can be found from Eq. (36), when utilizing the model for the relative particle-fluid velocity that was developed by Haugen et al. [30]. Furthermore, for the upper orange dashed line, the value of  $A_1A_2$  used in Eq. (48) is given by  $A_1A_2 = 0.08 + St/3$ , which is taken from Haugen et al. [30]. For comparison, the light blue lower dashed line has been obtained by using  $A_1A_2 = 0.2$ . It can be seen that the qualitative behaviour of Eq. (51) is fairly similar to the results from the DNS. The model for  $A_1A_2$  as found by Haugen et al. [30], yields a surprisingly good result, even though the physics in their case was more simplified and only mass transfer was considered. This supports the assumption that it is primarily the mass transfer effect that is influenced by the turbulence. We do believe though, that the discrepancy between the simulation results and the model results (orange upper dashed line) is due to the effect of the turbulence on the heat transfer. Finally, it could also be noted that a higher Damköhler number yields a higher variance in the Sherwood correction factor, while the variance is fairly small for the smaller **Da**.

### 5.2. The distribution of oxygen and temperature in the domain

Figure 12 shows the instantaneous value of the oxygen mass fraction in a slice of the domain when the mean oxygen mass fraction is 15% for three cases with increasing **Da** from left to right. A distinct increase in the difference between the

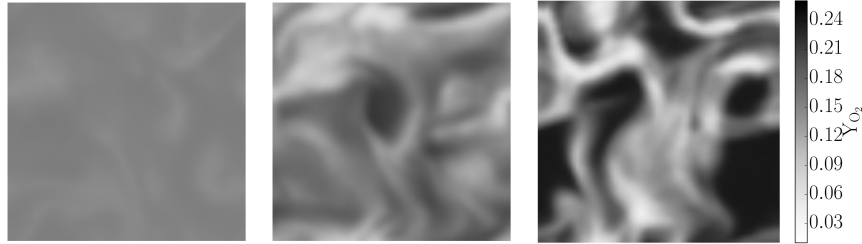


Figure 12: Plots of the oxygen mass fraction for cases with increasing  $\mathbf{Da}$ , 0.01, 0.09 and 1.00 from left to right,  $\bar{Y}_{O_2} = 15\%$ , the time of the snapshots is 100ms, 6ms and 2ms from left to right.

oxygen rich and lean regions is clearly visible for higher  $\mathbf{Da}$ . A high Damköhler number results in a large variance in the oxygen mass fraction, as clusters become depleted of oxygen in a short time, while the regions with low particle number density are left nearly untouched. This effect can be observed in Fig. (13), where a scatter plot of the normalized particle number density as a function of the oxygen mass fraction is shown. The low Damköhler case shows very similar levels of oxygen content for all particle number densities, while the large Damköhler case shows a clear correlation between high relative particle number densities and low oxygen content. In Fig. (14) the corresponding PDF of the oxygen mass fraction is shown. The constrained probabilities for regions where the particle number density is higher than its mean value,  $n_p > \bar{n}_p$  (dashed line in Fig. (13)), have different positions in the overall distribution. While the constrained distribution for low  $\mathbf{Da}$  fills nearly the full range of values of the unconstrained one, the constrained distribution for the large Damköhler case only covers the lower half of the unconstrained range of values. The values of oxygen mass fraction have a larger spread for higher  $\mathbf{Da}$ . Note that the mean oxygen mass fraction for all cases at the time of the snapshot was around 15%, hence the data is from different times (see Fig. (8)).

Finally the effect of turbulence on the temperature distribution in the domain is studied. The normalized particle number density is plotted as a function of the gas temperature in Fig. (15), and the resulting PDF of the gas temperature is shown in Fig. (16). The mean oxygen mass fraction is 15% for all cases. A higher Damköhler number simulation has a wider range of temperatures and a lower mean temperature than simulations of lower  $\mathbf{Da}$ . The lower mean temperature of the high Damköhler cases is explained by the high number of particles in the domain, which constitute a higher fraction of the energy stored in the particles, and an increase in radiation losses from the sum of all particles. The wide range

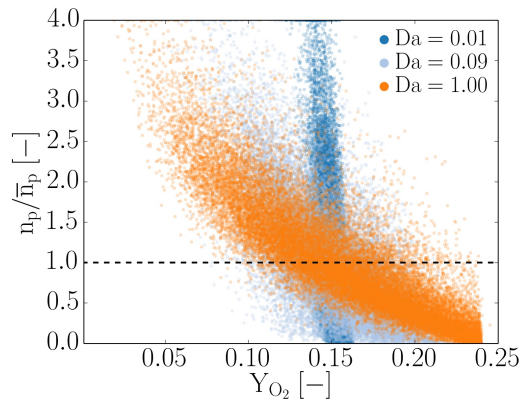


Figure 13: Scatter plot of the particle number density over the oxygen mass fraction. The mean oxygen mass fraction is  $\bar{Y}_{O_2} = 15\%$  for all three simulations.

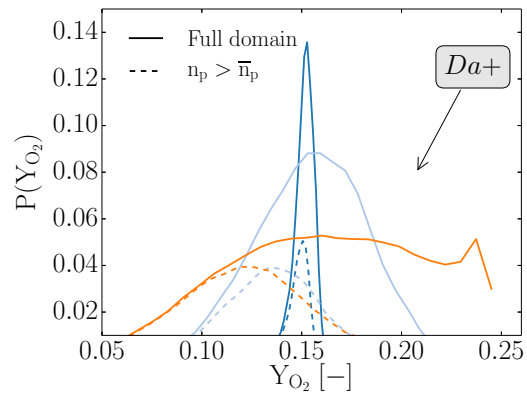


Figure 14: PDF of the oxygen mass fraction for the full domain (continuous lines) and in regions where  $n_p > \bar{n}_p$  (dashed lines). Higher  $Da$  result in broader distributions.

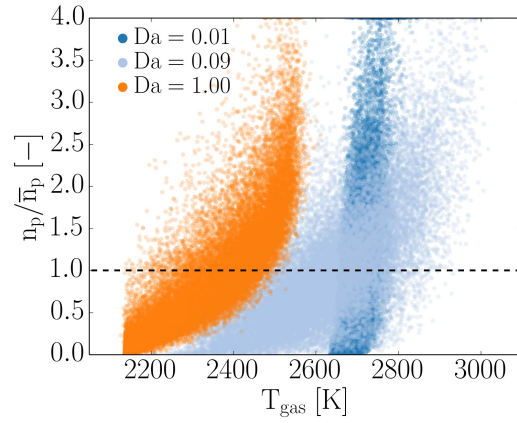


Figure 15: Scatter plot of the particle number over the domain temperature density.

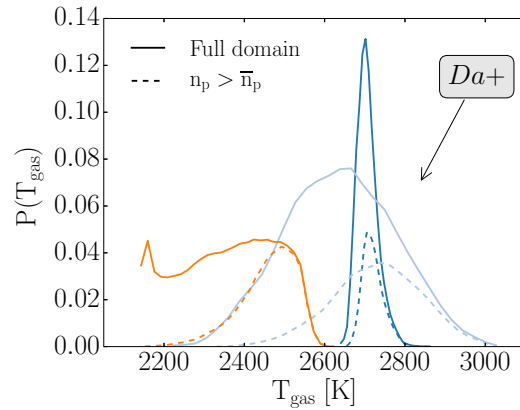


Figure 16: PDF of the domain temperature for cases with three different  $Da$ . The dashed line represents the subset of the domain where  $n_p > \bar{n}_p$ .

of temperatures found for medium  $\mathbf{Da}$  is believed to be due to the wide range of states the gas can be in. For medium  $\mathbf{Da}$ , parts of the domain have already been emptied of oxygen and cooled down, while other parts have not yet been in contact with particles.

## 6. Conclusions

The simple model of Haugen et al. [30] and Krüger et al. [29], where DNS was used to analyse heterogeneous reactions in isotropic turbulence, has been extended to incorporate real species and temperature effects. It has been found that the particles form clusters because of the turbulence. Treating the reactions for high  $\mathbf{Da}$  as only occurring on the outer shell of these particle clusters is found to give reasonable results, and a cluster dependent reaction rate  $\alpha_{cl}$  is found to yield a good approximation of the maximum rate of reaction that can be achieved for heterogeneous reactions. Haugen et al. [30] has given an approximate value of  $A_1A_2$ , which fits the results reasonably well. The fitting factors  $A_1$  and  $A_2$  are factors relating to the number density and surface-to-volume ratio of the particle clusters, both of which depend on the shape of the clusters. Predicting the shape of the particle clusters, and thus values of  $A_1$  and  $A_2$  from flow field and particle properties is the topic of ongoing work. The simulations show the same trend as obtained in the work of Haugen et al. [30] and Krüger et al. [29]. However, using  $A_1A_2 = 0.08 + St/3$  slightly overpredicts the reaction rate for low and medium  $\mathbf{Da}$ . For low and intermediate  $\mathbf{Da}$ , a good fit is achieved with  $A_1A_2 = 0.2$ , at the cost of underprediction for higher  $\mathbf{Da}$ . The developed model, as presented in Eq. (51), should be used in RANS simulations to account for the effect of turbulence on the conversion of heterogeneously reacting particles. The model accounts both for 1) the effect of increased mass transfer due to turbulence-induced relative velocities between particles and fluid, and 2) the effect of particle clustering.

The reason for the discrepancies between the results obtained in this work and the results of Haugen et al. [30] are thought to be due to the thermal and kinetic effects that have been included in the current work. In the work of Haugen et al. [30], the consumption of a passive scalar is studied, which does not influence the carrier fluid. Meanwhile, the consumption of oxygen directly affects the density, temperature, composition and momentum of the fluid. Another difference is the lower flow Reynolds number of approximately 40 that has been studied here, while the work of Haugen et al. studies flows with Reynolds numbers in the range of 80-2200.



The Sherwood correction factor is also dependent on the size ratio of the particles and the grid cells size, which are all factors that influence the cost of the simulations. The ratio of particle to grid cell size in the present work was chosen so that the reaction rates at small  $Da$  behave similar to the homogeneous assumption at reasonable cost and ensure the validity of the point-particle assumption. Increasing the particle size will yield lower Sherwood correction factors. In addition, it tends to yield numerical instabilities.

It is worth noting that extending this analysis to include several heterogeneous and homogeneous reactions will complicate the interpretation of the effect of turbulence. Interestingly, this can result in cases where production/consumption of one species can be modelled by the homogeneous approach, while other species' reactions are happening at the cluster dependent reaction rate.

The proposed model gives a good approximation of the char consumption rate in reacting flows with heterogeneous reactions. To further improve its predictability, more work has to be done to identify an appropriate correlation for  $A_1A_2$ , and to analyse the effect of several heterogeneous and homogeneous reactions, especially for cases where non-unimolar reactions are considered. The effects of particle heating and heat transfer between fluid and particles should also be examined.

## Acknowledgements

The research leading to these results has received funding from the Polish-Norwegian Research Programme operated by the National Centre for Research and Development under the Norwegian Financial Mechanism 2009-2014 in the frame of Project Contract No Pol-Nor/232738/101/2014.

## References

### References

- [1] N. Hashimoto, H. Watanabe, Numerical analysis on effect of furnace scale on heat transfer mechanism of coal particles in pulverized coal combustion field, *Fuel Processing Technology* 145 (2016) 20 – 30. doi:<http://dx.doi.org/10.1016/j.fuproc.2016.01.024>.  
URL <http://www.sciencedirect.com/science/article/pii/S0378382016300236>

- [2] G. Olenik, O. Stein, A. Kronenburg, LES of swirl-stabilised pulverised coal combustion in IFRF furnace no. 1, *Proceedings of the Combustion Institute* 35 (3) (2015) 2819 – 2828. doi:<http://dx.doi.org/10.1016/j.proci.2014.06.149>.  
URL <http://www.sciencedirect.com/science/article/pii/S1540748914003071>
- [3] J. H. Chen, A. Choudhary, B. de Supinski, M. DeVries, E. R. Hawkes, S. Klasky, W. K. Liao, K. L. Ma, J. Mellor-Crummey, N. Podhorszki, R. Sankaran, S. Shende, C. S. Yoo, Terascale direct numerical simulations of turbulent combustion using s3d, *Computational Science & Discovery* 2 (1) (2009) 015001.  
URL <http://stacks.iop.org/1749-4699/2/i=1/a=015001>
- [4] J. Kim, P. Moin, R. Moser, Turbulence statistics in fully developed channel flow at low reynolds number, *J. Fluid Mech* 177 (1987) 133–166.
- [5] D. Veynante, L. Vervisch, Turbulent combustion modeling, *Progress in Energy and Combustion Science* 28 (3) (2002) 193 – 266. doi:[http://dx.doi.org/10.1016/S0360-1285\(01\)00017-X](http://dx.doi.org/10.1016/S0360-1285(01)00017-X).  
URL <http://www.sciencedirect.com/science/article/pii/S036012850100017X>
- [6] T. Poinso, D. Veynante, *Theoretical and Numerical Combustion*, Poinso and Veynante, 2012.
- [7] D. Spalding, Mixing and chemical reaction in steady confined turbulent flames, *Proceedings of the Combustion Institute* (1971) 649–657.
- [8] S. B. Pope, Pdf method for turbulent reacting flows., *Progr. Energy Combustion Sci.* 11 (1985) 119–95.
- [9] K. Bray, J. Moss, A unified statistical model of the premixed turbulent flame, *Acta Astronautica* 4 (3) (1977) 291 – 319. doi:[http://dx.doi.org/10.1016/0094-5765\(77\)90053-4](http://dx.doi.org/10.1016/0094-5765(77)90053-4).  
URL <http://www.sciencedirect.com/science/article/pii/S0094576577900534>
- [10] S. Pope, The evolution of surfaces in turbulence, *International Journal of Engineering Science* 26 (5) (1988) 445 – 469.

doi:[http://dx.doi.org/10.1016/0020-7225\(88\)90004-3](http://dx.doi.org/10.1016/0020-7225(88)90004-3).

URL <http://www.sciencedirect.com/science/article/pii/S0020722588900043>

- [11] A. R. Kerstein, W. T. Ashurst, F. A. Williams, Field equation for interface propagation in an unsteady homogeneous flow field, *Phys. Rev. A* 37 (1988) 2728–2731. doi:10.1103/PhysRevA.37.2728.  
URL <http://link.aps.org/doi/10.1103/PhysRevA.37.2728>
- [12] S. Burke, T. Schumann, Diffusion flames, *Industrial & Engineering Chemistry* 20 (1928) 998–1004.
- [13] B. Magnussen, B. Hjertager, On mathematical models of turbulent combustion with special emphasis on soot formation and combustion, *Proceedings of the Combustion Institute* 16 (1) (1979) 719729.
- [14] A. Y. Klimenko, Multicomponent diffusion of various admixtures in turbulent flow, *Fluid Dynamics* 25 (3) (1990) 327–334. doi:10.1007/BF01049811.  
URL <http://dx.doi.org/10.1007/BF01049811>
- [15] R. W. Bilger, , *Physics of Fluids A: Fluid Dynamics* 5 (2) (1993) 436–444. doi:10.1063/1.858867.  
URL <https://doi.org/10.1063%2F1.858867>
- [16] N. Peters, Laminar flame concepts in turbulent combustion, *Proceedings of the Combustion Institute* 21 (1986) 1231–50.
- [17] M. L. de Souza-Santos (Ed.), *Solid Fuels Combustion and Gasification*, CRC Press, 2010. doi:10.1201/9781420047509.
- [18] A. Eaton, L. Smoot, S. Hill, C. Eatough, Components, formulations, solutions, evaluation, and application of comprehensive combustion models, *Progress in Energy and Combustion Science* 25 (4) (1999) 387 – 436. doi:[http://dx.doi.org/10.1016/S0360-1285\(99\)00008-8](http://dx.doi.org/10.1016/S0360-1285(99)00008-8).  
URL <http://www.sciencedirect.com/science/article/pii/S0360128599000088>
- [19] W. E. Ranz, W. R. Marshall, Evaporation from drops, *Chemical Engineering Progress* 48 (1952) 141–146.

- [20] J. K. Eaton, J. R. Fessler, Preferential concentration of particles by turbulence, *International Journal of Multiphase Flow* 20 (1994) 169–209.
- [21] A. M. Wood, W. Hwang, J. K. Eaton, Preferential concentration of particles in homogeneous and isotropic turbulence, *International Journal of Multiphase Flow* 31 (2005) 1220–1230.
- [22] J. Bec, Fractal clustering of inertial particles in random flows, *Physics of Fluids* 15 (11) (2003) L81–L84. doi:<http://dx.doi.org/10.1063/1.1612500>.  
URL <http://scitation.aip.org/content/aip/journal/pof2/15/11/10.1063/1.1612500>
- [23] K. Annamalai, S. Ramalingam, Group combustion of char carbon particles, *Combustion and Flame* 70 (3) (1987) 307–332. doi:10.1016/0010-2180(87)90111-8.
- [24] J. Reveillon, F. Demoulin, Evaporating droplets in turbulent reacting flows, *Proceedings of the Combustion Institute* 31 (2) (2007) 2319 – 2326. doi:<http://dx.doi.org/10.1016/j.proci.2006.07.114>.  
URL [//www.sciencedirect.com/science/article/pii/S1540748906001222](http://www.sciencedirect.com/science/article/pii/S1540748906001222)
- [25] K. Luo, H. Wang, J. Fan, F. Yi, Direct Numerical Simulation of Pulverized Coal Combustion in a Hot Vitiated Co-flow, *Energy & Fuels* 26 (10) (2012) 6128–6136. doi:10.1021/ef301253y.
- [26] T. Hara, M. Muto, T. Kitano, R. Kurose, S. Komori, Direct numerical simulation of a pulverized coal jet flame employing a global volatile matter reaction scheme based on detailed reaction mechanism, *Combustion and Flame* 162 (12) (2015) 4391 – 4407. doi:<http://dx.doi.org/10.1016/j.combustflame.2015.07.027>.  
URL <http://www.sciencedirect.com/science/article/pii/S001021801500228X>
- [27] T. Brosh, N. Chakraborty, Effects of equivalence ratio and turbulent velocity fluctuation on early stages of pulverized coal combustion following localized ignition: A direct numerical simulation analysis, *Energy and Fuels* 28 (2014) 6077–6088.

- [28] T. Brosh, D. Patel, D. Wacks, N. Chakraborty, Numerical investigation of localised forced ignition of pulverised coal particle-laden mixtures: A direct numerical simulation (dns) analysis, *Fuel* 145 (2015) 50–62.
- [29] J. Krüger, N. E. Haugen, D. Mitra, T. Løvås, The effect of turbulent clustering on particle reactivity, *Proceedings of the Combustion Institute* (2016) –doi:<http://dx.doi.org/10.1016/j.proci.2016.06.187>.  
URL <http://www.sciencedirect.com/science/article/pii/S1540748916302498>
- [30] N. E. Haugen, J. Krüger, D. Mitra, T. Løvås, The effect of turbulence on mass and heat transfer rates of small inertial particles. doi:arXiv:1701.04567v1.  
URL <https://arxiv.org/abs/1701.04567>
- [31] M. B. Tilghman, R. E. Mitchell, Coal and biomass char reactivities in gasification and combustion environments, *Combustion and Flame* 100 (2014) 100–101.
- [32] M. B. Tilghman, N. E. L. Haugen, R. E. Mitchell, A comprehensive char-particle gasification model adequate for entrained-flow and fluidized-bed gasifiers, *Energy & Fuels* doi:10.1021/acs.energyfuels.6b02148.
- [33] L. Chen, S. Z. Yong, A. F. Ghoniem, Oxy-fuel combustion of pulverized coal: Characterization, fundamentals, stabilization and CFD modeling, *Progress in Energy and Combustion Science* 38 (2) (2012) 156–214. doi:10.1016/j.pecs.2011.09.003.
- [34] A. Brandenburg, Pencil code homepage (July 2014).  
URL <http://pencil-code.nordita.org/>
- [35] J. Williamson, Low-storage runge-kutta schemes, *Journal of Computational Physics* 35 (1) (1980) 48 – 56. doi:[http://dx.doi.org/10.1016/0021-9991\(80\)90033-9](http://dx.doi.org/10.1016/0021-9991(80)90033-9).  
URL <http://www.sciencedirect.com/science/article/pii/S0021999180900339>
- [36] N. Babkovskaia, N. Haugen, A. Brandenburg, A high-order public domain code for direct numerical simulations of turbulent combustion, *Journal of Computational Physics* 230 (1) (2011) 1 – 12. doi:<http://dx.doi.org/10.1016/j.jcp.2010.08.028>.

URL <http://www.sciencedirect.com/science/article/pii/S0021999110004754>

- [37] A. Brandenburg, The inverse cascade and nonlinear alpha-effect in simulations of isotropic helical hydromagnetic turbulence, *The Astrophysical Journal* 550 (2) (2001) 824.  
URL <http://stacks.iop.org/0004-637X/550/i=2/a=824>
- [38] N. E. L. Haugen, M. B. Tilghman, R. E. Mitchell, The conversion mode of a porous carbon particle during oxidation and gasification, *Combustion and Flame* 161 (2) (2014) 612 – 619. doi:<http://dx.doi.org/10.1016/j.combustflame.2013.09.012>.  
URL <http://www.sciencedirect.com/science/article/pii/S0010218013003441>
- [39] S. Sundaram, L. R. Collins, Numerical considerations in simulating a turbulent suspension of finite-volume particles, *Journal of Computational Physics* 124 (2) (1996) 337 – 350. doi:<http://dx.doi.org/10.1006/jcph.1996.0064>.  
URL <http://www.sciencedirect.com/science/article/pii/S0021999196900649>
- [40] K. D. Squires, J. K. Eaton, Particle response and turbulence modification in isotropic turbulence, *Physics of Fluids* 7 (1990) 1191–12–3.
- [41] S. Elghobashi, G. C. Truesdell, On the two-way interaction between homogeneous turbulence and dispersed solid particles. i: Turbulence modification., *Physics of Fluids A* 5 (1993) 1790–1801.
- [42] N. E. L. Haugen, R. E. Mitchell, M. B. Tilghman, A comprehensive model for char particle conversion in environments containing O<sub>2</sub> and CO<sub>2</sub>, *Combustion and Flame* 162 (4) (2015) 1455 – 1463. doi:<http://dx.doi.org/10.1016/j.combustflame.2014.11.015>.  
URL <http://www.sciencedirect.com/science/article/pii/S0010218014003575>
- [43] C. T. Crowe, J. D. Schwarzkopf, M. Sommerfeld, Y. Tsuji, *Multiphase Flows Droplets*, CRC Press, 2012.
- [44] M. M. Baum, P. J. Street, Predicting the combustion behaviour of coal particles, *Combustion Science and Technology* 3 (5) (1971)

231–243. arXiv:<http://dx.doi.org/10.1080/00102207108952290>,  
doi:10.1080/00102207108952290.  
URL <http://dx.doi.org/10.1080/00102207108952290>

- [45] K. Li, C. You, Particle combustion model simultaneously considering a volatile and carbon reaction, *Energy & Fuels* 24 (2010) 4178–4184.